Available online at www.sciencedirect.com
ScienceDirect
Trans. Nonferrous Met. Soc. China 34(2024) 255−264
Transactions of Nonferrous Metals Society of China
www.tnmsc.cn

Mechanical and energy absorption properties of multilayered ultra-light sandwich panels produced by 3D-printing and electroforming

Mehrnoosh HOSSEINPOUR, Salar ROHANI NEJAD, Seyed Mohammad Hossein MIRBAGHERI

Department of Materials and Metallurgical Engineering,
Amirkabir University of Technology, Hafez St., Tehran, 15875-4413, Iran

Received 6 August 2022; accepted 16 December 2022

Abstract: This investigation aims to assess the mechanical and energy absorption properties of the light sandwich panel portions made of open-cell polymer and metal/polymer foam cores. These multi-layered sandwich panels were produced by additive manufacturing of polymeric resin and electrodeposition of three layers of metals, Ni/Ni−Cu/Ni, with 4, 5, and 6 pores per inch (PPI). The yield strength, energy absorption density, complementary energy, and specific energy absorption (SEA) were measured during uniaxial compression deformation. The results indicate that compared with pure Ni and Cu sandwich panel portions with the same thickness, the abovementioned properties of the sandwich panels had a noteworthy improvement. Mechanical and energy absorption properties were improved by increasing the PPI and the presence of metallic layers. In a sandwich panel with 6 PPI, the yield strength (energy absorption density) was improved from 0.12 MPa (0.12 MJ/m^3) for the polymeric sandwich panel to 1.83 MPa (0.67 MJ/m^3) for the metallic sandwich panel. Investigations on normalized energies of these structures show a predictable behavior for these sandwich panels during plastic deformations. The results show that the multi metallic layers improved the mechanical behavior of these novel sandwich panels. Noticeable enhancement of the calculated properties of these advanced materials guarantees their unique application in variable industries.

Key words: sandwich panel; energy absorption; metal foam; Voronoi structures; additive manufacturing; electroforming of metal

1 Introduction

Sandwich panels regarded with their unique properties such as outstanding energy absorption, impact resistance, compressive strength, stiffness, specific strength, and economic issues find their place in automotive, aerospace, marine, naval, and building construction industries [1−3]. Sandwich panels can be categorized as synthetic fiber base, natural fiber base, and metal base regarding their applications. Metal base sandwich panels have gained significant importance and attention among these three types during the latest decade [1]. Recently, honeycomb, open and close cell metal foams, corrugated plates, trusses, and Y-frame have been applied to core trends [2,4−7]. Parameters such as type of core design, thickness, dimension, material type, and how to use adhesive material play an essential role in the performance of sandwich panels [1,2].

According to researches published in the Journal of Sandwich Structures and Materials during 2015−2020 just under 40% of researchers prefer foams as a prominent core design [1]. Open-cell metal foams can be a promising core due to their low density [8], interconnected pores, high surface-to-volume ratio, and excellent specific

Corresponding author: Seyed Mohammad Hossein MIRBAGHERI, E-mail: smhmirbagheri@aut.ac.ir
DOI: 10.1016/S1003-6326(23)66396-4

strength [9]. The characteristics of the open-cell foam core, such as strut length and relative density, significantly affect the compressive strength and buckling phenomenon [7,10−16]. Ni−Cu alloys and structural combinations are used in many engineering applications such as sandwich panels due to their usability in high strain rates and mechanical characterization [17−19].

In the present study, an integrated metal/polymer sandwich panel portion was produced by fabricating a polymeric precursor through 3D printing and electrodeposition of metal. The effect of pore density (pores in inch, PPI) and CAD seed on the mechanical behavior and energy absorbing properties of these sandwich panel portions was investigated. Elastic properties of the 3D-printed resin precursor combined with the mechanical and energy-absorbing properties of the Ni−Cu coat indicate significant mechanical and energy absorption properties as a metal/polymer sandwich panel. The low production cost and the option to control the final material properties lead to a new sandwich panel in energy absorption applications.

2 Experimental

The multi-layer Ni/Ni−Cu/Ni sandwich panel portions were produced by 3D printing and electroforming to investigate the effect of PPI on mechanical and energy absorption properties of these multi-layer metal foam as a possible core for wide sandwich panels. Figure 1 shows a schematic of the production.

2.1 Production of a portion of sandwich panel

The modeling was based on an algorithm of Grasshopper in Rhinoceros software and the distribution of seed numbers which act as nodes where struts come together. The metal foam CAD model of the present study was obtained from an integrated volume by connecting the cavities and shaping a porous media. After modeling the foam core, the upper and lower plates with thickness of 1.5 mm connected to the core as an integrated sandwich panel portion. The physical properties of foams can be seen in Table 1.

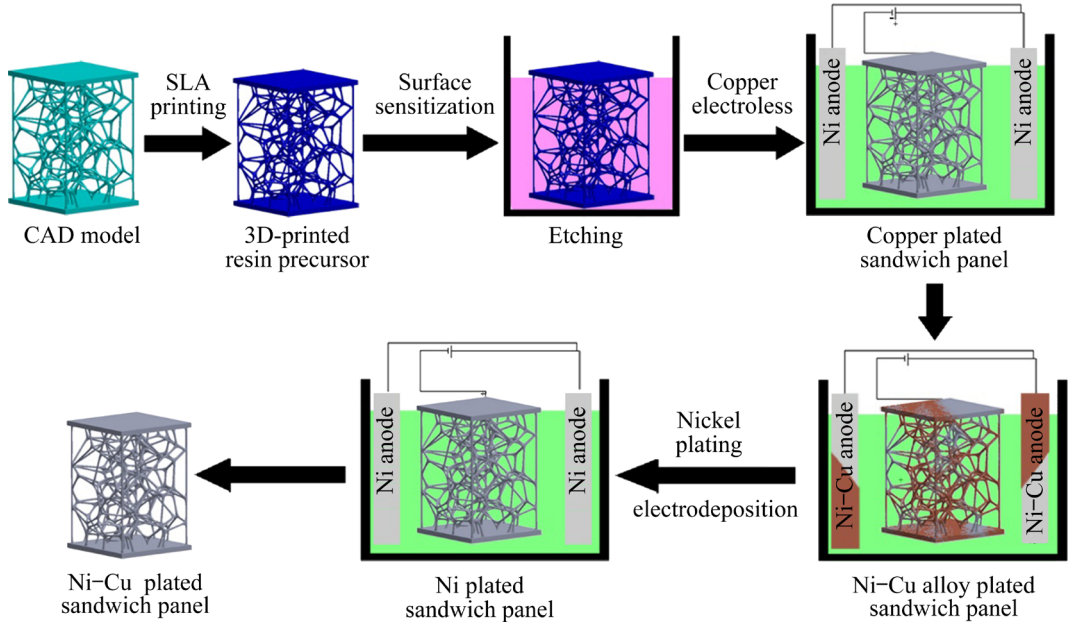

Fig. 1 Schematic of production method of multi-layer sandwich panel portions

Table 1 Parameters of 3D-RP and 3D-ML with different PPI

Parameter	3D-RP			3D-ML		
	4 PPI	5 PPI	6 PPI	4 PPI	5 PPI	6 PPI
Seed number	35	45	55	35	45	55
Surface area/mm^2	5741	8059	10357	5741	8059	10357
Mass/g	2.69	3.58	4.15	10.97	11.21	11.53
Pore fraction/vol.%	0.91	0.88	0.84	0.91	0.88	0.84

The modeling was followed by the 3D printing of polymeric sandwich panel by Anycubic Photon Mono X LCD resin printer with eSUN tough resin in three different PPIs of 4, 5, and 6. These polymeric sandwich panel portions are named 3D-RP which is shown in Fig. 2(a). Due to creating the suitable surface for the physical absorption of the metallic layers, the 3D-RP was first immersed in an alkaline solution. After the electroless process, first Ni layer appeared through the electrochemical deposition process in sulfamate solution. This process lasted for 4 h. In the next step, the Ni-electroformed 3D-RP was electroformed for 1 h with a Ni−Cu alloy electroforming anode to reach the second layer (Ni−Cu alloy layer). The final sandwich panel portion was reached after Ni electroforming for 1 h. Multi-layer (Ni/Ni−Cu/Ni) sandwich panel portions are presented in Fig. 2(b). These metal sandwich panel portions are symbolled 3D-ML, produced in 4, 5, and 6 PPI and called 3D-ML-4, 3D-ML-5, and 3D-ML-6, respectively.

2.2 Experiments

The compression test was designed based on ISO 13314 standard [20] for flat porous materials. The Instron machine with a 5 t capacity and the applied load rate of 0.013 s^{-1} was used to evaluate the compressive behavior of 3D-RP and 3D-ML sandwich panel portions at room temperature. Microstructural images and EDS line scans were taken by field emission electron microscope (FE-SEM) with a resolution of 1.5 nm at 15 kV and 4.5 nm at 1 kV.

3 Results and discussion

In the present study, the compressive behavior, fracture mechanism, the energy absorption properties, energy absorption efficiency, and the normalized energies of multi-layer sandwich panels have been investigated.

3.1 Compressive behavior and fracture mechanism

The compression sequences are shown in Fig. 3. Compared to pure Ni foam cores, 3D-ML sandwich panel showed softer failures and did not crush with the intensity of Ni foam cores because of the strengthening due to alloying of Ni/Cu layer. The fracture in the 3D-ML sandwich panels was more ductile than that in the Ni foam cores. The initial failures occurred at an angle of about 45° (after 5% of strain). Then, the 3D-ML gradually crushed down, lost its strength, and became denser.

Figure 4 shows the FE-SEM images of the 3D-ML-6 after the compression test. According to Fig. 4(a), the thickness of the reinforcement layer is

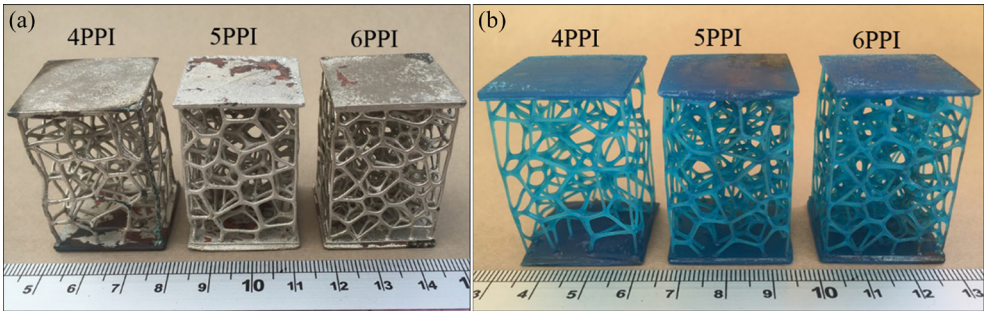

Fig. 2 3D-printed precursors with different PPI (a), and electroplated precursors (b)

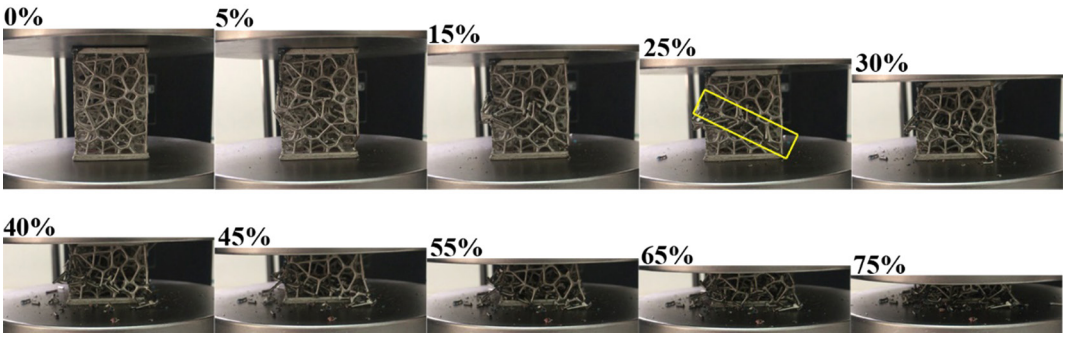

Fig. 3 Pictures of 3D-ML-6 during compression test based on ISO 13314

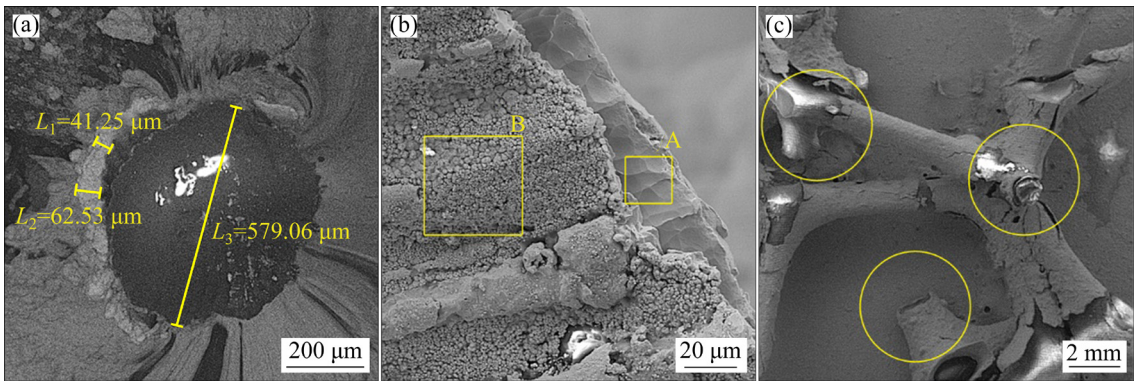

Fig. 4 SEM images of 3D-ML-6 after compression test: (a) Thicknesses of layer and dimension of 3D-printed structure; (b) Demonstration of multi-layer properties of foams; (c) Fracture mechanism hypothesis

about 40−60 μm. Figure 4(b) illustrates the layers of the metal foam core. The Zone A depicts the first Ni layer, and the Zone B shows the electroless layer of Cu, which is the primer layer of the first Ni deposited layer. Buckling is the primary phenomenon and reason for the structure collapse. According to Fig. 4(c), Ni/Ni−Cu/Ni multi-layer reinforcement caused an improvement in controlling buckling phenomena by moving the fracture interface to the nodes. This hypothesis is based on the less elastic nature of metallic shells compared to resin polymers. These nodes preserved their structure until the final stages of the compression test due to their robust nature.

This improvement in mechanical behavior is due to the solid solution alloying and the stiffness of the multilayer shell. As shown in Fig. 4(c), it is clear that the metal shells near to the fractured sections (node) is peeled off from the 3D-RP substrate because of the geometry stiffness of nodes. Furthermore, the micro-cracks nucleate around nodes and grow in the axis of struts of the 3D-ML cores. The micro diffusion bond between the metallic layer was detected by the line scan with FE-SEM and presented in Fig. 5. According to the line scan in Fig. 5(b), Cu and Ni have diffused approximately 30 μm at the interface of the second and third layers.

The force−displacement curves were obtained from the compression test and transformed into stress−strain diagrams shown in Fig. 6. The reinforcement layers and increasing PPI (decreasing the strut length) control the buckling phenomenon, increase the enduring forces, and increase the tolerated stresses. According to Fig. 6(b), the stress−strain diagram of these sandwich panels has three regions.

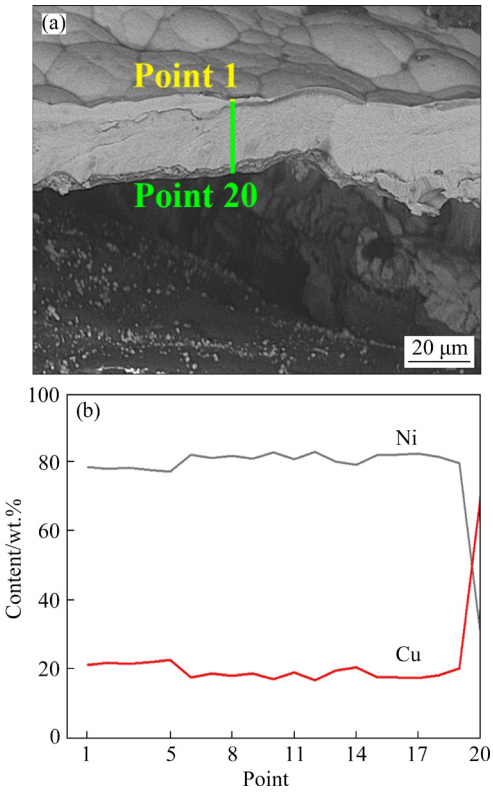

Fig. 5 EDS line scan of 3D-ML-6: (a) Area of scanning; (b) Contents of Ni and Cu concerning scanning points

Region I is the first tolerated stresses which contain a first massive rise in stress values and is called the first maximum compressive strength [20] (yield strength). This part is the start of deformation, and the first fractures happen after the highest value of stresses in this section of the diagram. Region II is a plateau zone, and it contains internal (node) fractures of the metallic core of the sandwich panel. Finally, the diagram reaches Region III, which is the densification of the 3D-ML cores. Figure 6(d) compares the best sample of the present study with its Ni foam core compatriot. According to Fig. 6(d),

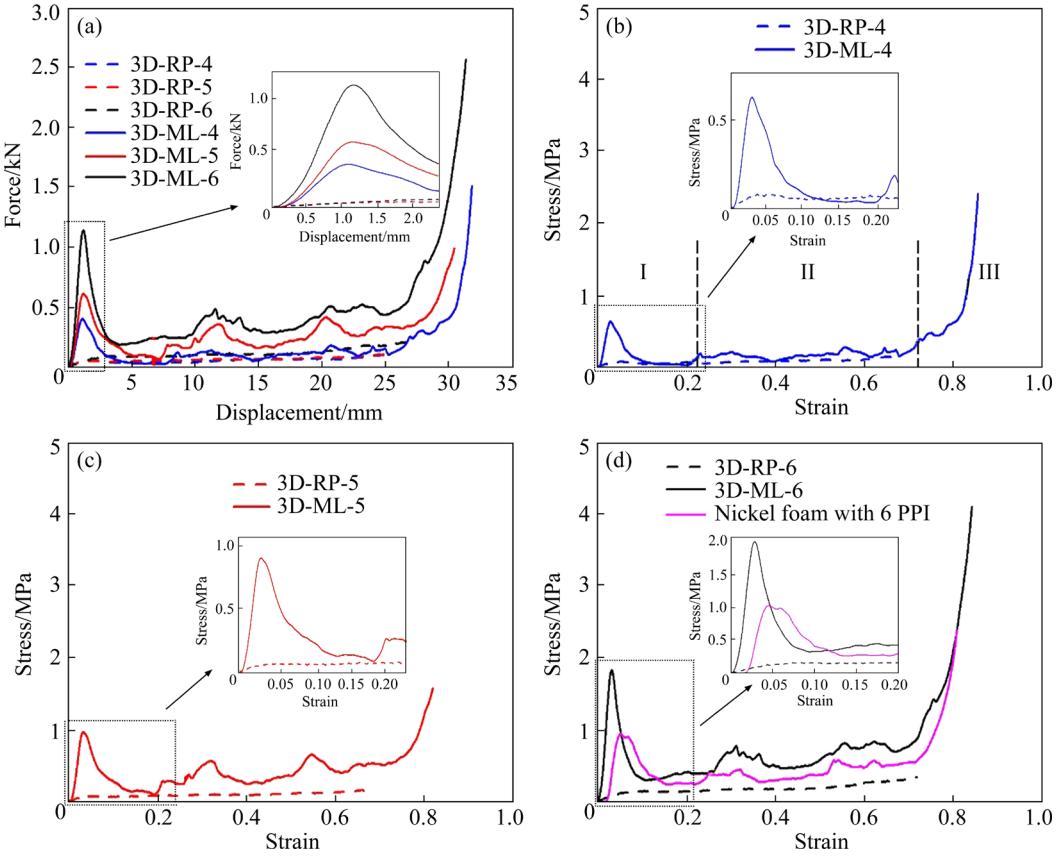

Fig. 6 Force−displacement curve obtained from compression test (a) and stress−strain curves of sandwich panel portions (b−d): (b) 4 PPI; (c) 5PPI; (d) 6 PPI

there is egregious difference between 3D-ML and Ni core, and the 3D-ML-6 tolerates much higher stresses with the same topology.

3.2 Yield strength

According to Standard ISO 13314, yield stress is the highest amount of tolerated stress in the first stage of the stress−strain diagrams. According to Fig. 6, increasing the PPI and the presence of metallic layers improved yield strength. By comparing 3D-RP-6 and 3D-ML-6, this parameter was improved from 0.12 to 1.83 MPa (14 times), and by comparing 3D-ML-5 and 3D-ML-6, it was increased from 0.97 to 1.83 MPa (2 times), which is a significant improvement for any engineering material. It is worth mentioning that the 3D-ML-6 compared to its Ni foam cores, was improved in this area for two times, which could be the effect of the Ni/Cu layer. Figure 7(a) shows the relation between specific strength with PPI. The specific strength is also an essential factor for porous structures. This factor is an ascending parameter for the reinforced structures too. By comparing 3D-ML-6 and 3D-ML-5, the specific strength has doubled.

The calculated stress results from applying force divided by the surface tolerating this force. However, how to choose this surface is very important and affects the final results. The common method is to select the upper plate surface area as the force-applied surface. The cross-sectional area of the core of sandwich structures that bears the applied force can be calculated through CAD software. It allows using of this area in stress calculation. This method can provide better and more realistic view of the amount of stress bore by the panel and the core of sandwich structures. The two panels transmit the force to the core (struts) of the sandwich panel during compression loading. These struts had borne more stresses at a constant applied force than the reported stresses using the surface area of panels due to the lower cross-sectional area. Three different cross-sections were considered, and the surface area of these sections is shown in Fig. 7(b). Three strain stress curves were presented based on these cross-section surface areas. Finally, calculated yield strength of each cross-section is presented in Fig. 7(b).

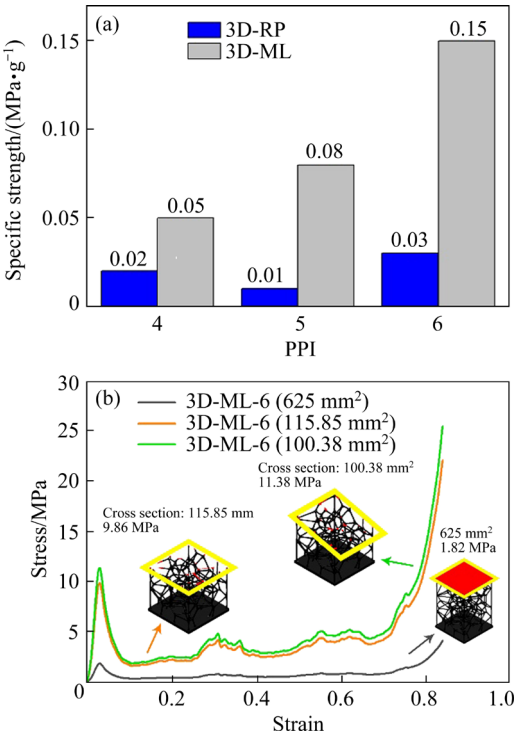

Fig. 7 Specific strength of structures in relation with PPI (a) and effect of cross section on stress strain (b)

3.3 Energy absorption behavior

The properties studied for the present sandwich panel portions are the absorbed energy, energy absorption efficiency, specific energy absorption, and normalized energy. The absorbed energy can be calculated in two ways. The first is the energy absorption (strain energy), and the second is the complementary energy. Both are calculated through Eqs. (1)−(3) [21−25]:

$$u=\frac{U}{V}=\int_0^x\frac{F\mathrm{d}x}{V}=\int_0^x\frac{F\mathrm{d}x}{AX_0}=\int_0^\varepsilon\sigma\mathrm{d}\varepsilon \quad (1)$$

$$u^*=\frac{U^*}{V}=\int_0^F\frac{x\mathrm{d}F}{V}=\int_0^F\frac{x\mathrm{d}F}{X_0A}=\int_0^\sigma\varepsilon\mathrm{d}\sigma \quad (2)$$

$$u_\mathrm{t}=u+u^*=\int\mathrm{d}(\sigma\cdot\varepsilon)=\int\sigma\mathrm{d}\varepsilon\int\varepsilon\mathrm{d}\sigma \quad (3)$$

where u_t is the total energy, and V is the volume of foams.

The energy absorption density and the complementary energy were obtained through Eqs. (1) and (2), respectively. Consequently, this calculation leads to the total energy, which is calculable by Eq. (3) [21−25]. All of these parameters are calculated and reported in Table 2.

3.4 Strain energy

The strain energy (U) represents the energy stored in a deformed body [26]. The energy absorption density (EAD) is obtained from the area under the force−displacement curve of the structures through Eq. (1), and is presented in Fig. 8.

Table 2 Energy parameters of 3D-ML and 3D-RP with different PPI

Energy parameter	3D-RP		
	4 PPI	5 PPI	6 PPI
Energy absorption density/(MJ·m^{-3})	0.06	0.07	0.12
Complementary strain energy/(MJ·m^{-3})	0.1	0.11	0.23
Total energy/(MJ·m^{-3})	0.16	0.18	0.35
Energy parameter	**3D-ML**		
	4 PPI	5 PPI	6 PPI
Energy absorption density/(MJ·m^{-3})	0.22	0.36	0.67
Complementary strain energy/(MJ·m^{-3})	2.06	1.29	3.46
Total energy/(MJ·m^{-3})	2.28	1.65	4.13

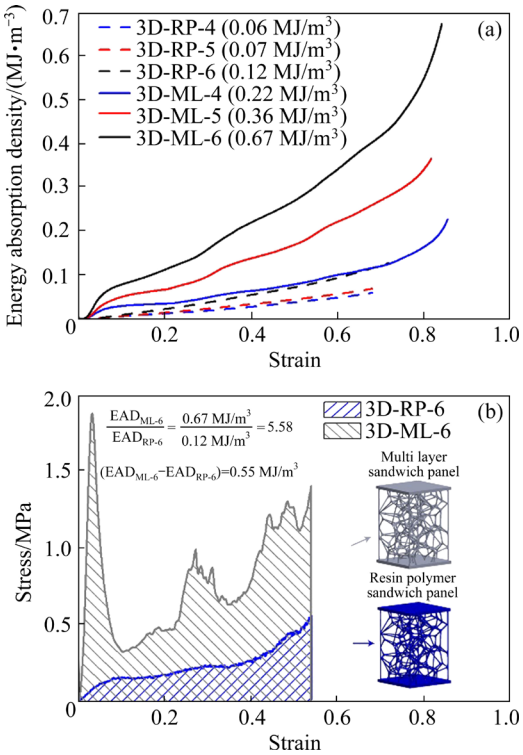

Fig. 8 Energy absorption density of sandwich structures concerning strain (a), and comparison of energy absorption density of strongest structures in each category (b)

According to Fig. 8(a), the increase in PPI and the presence of the reinforcement layer improved the energy absorption. By comparing 3D-RP-6 and 3D-ML-6, which are the strongest structures in each category, the energy absorption density increased by about four times.

3.5 Complementary strain

The complementary energy corresponds to the area above the stress−strain curve for a linearly elastic material. It is calculated by Eq. (2) and presented in Fig. 9.

The complementary strain is also positively affected by the metal reinforcement layer and grows significantly compared to the polymer samples. According to Eq. (3), sum of these two types of energy is the total energy and is presented in Table 2.

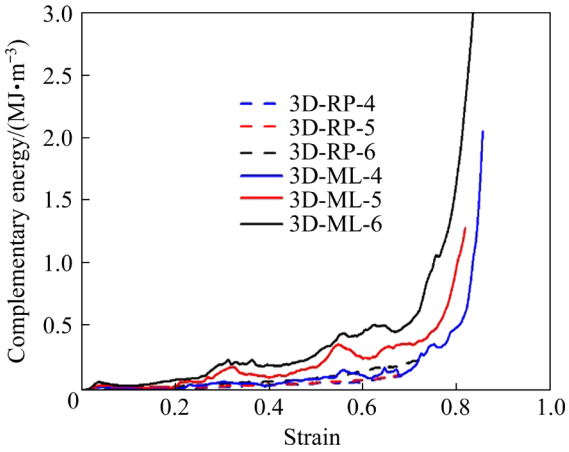

Fig. 9 Complementary strain concerning strain

3.6 Normalized energy

Equation (4) normalized the absorbed energies to reach a better and comparative factor [21−25]. This normalized parameter could be presented in two styles. The first concerns normalized stress, and the second concerns normalized strain, which is presented in Fig. 10.

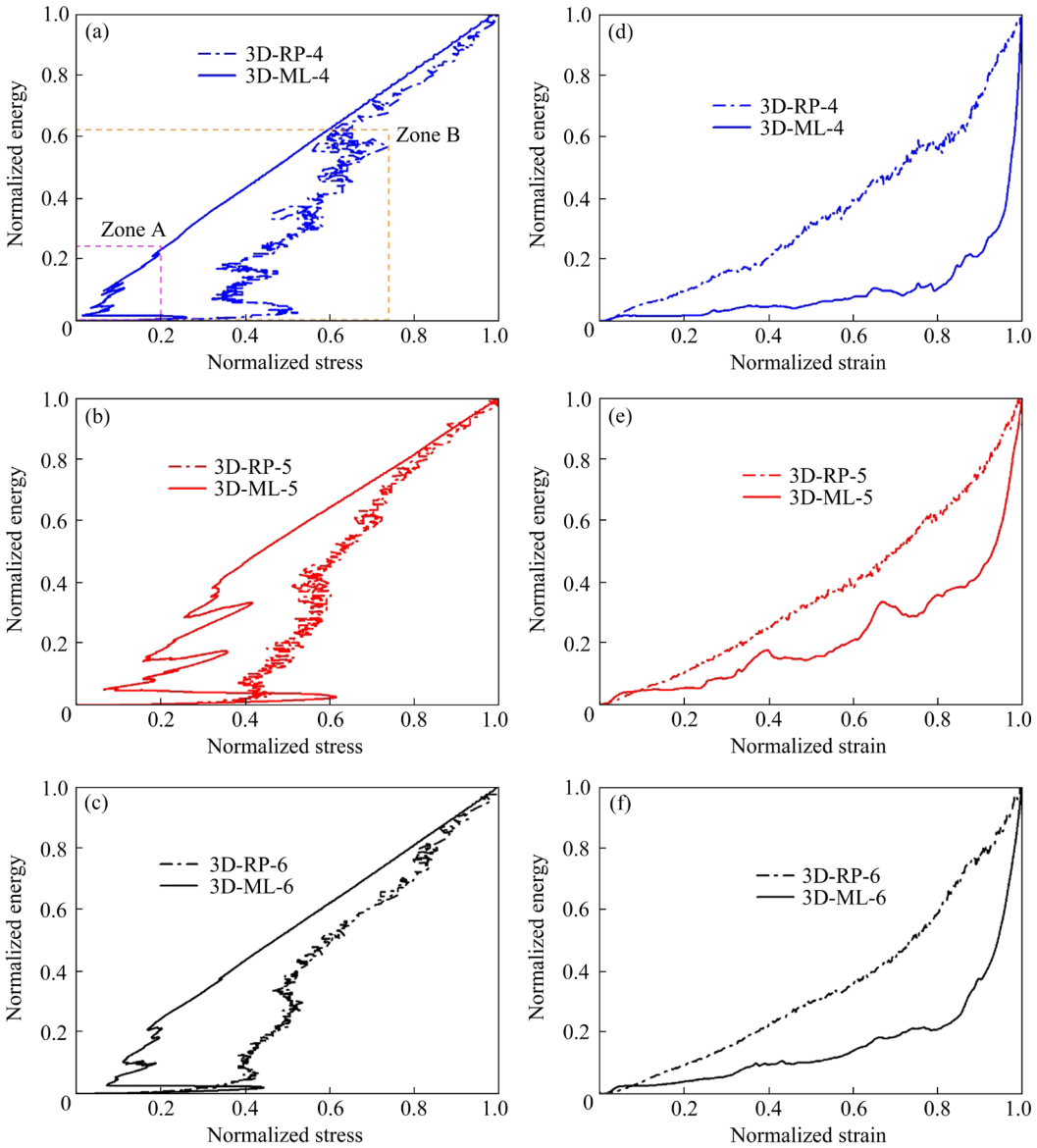

Fig. 10 Demonstration of normalized energy concerning normalized stress (a−c) and strain (d−f) separated by PPI

$$E_{\mathrm{N}}=\sum_{i=1}^{n}\frac{u_{t_i}}{\max[0,u_{t_i}]} \tag{4}$$

According to Fig. 10(a), the 3D-ML curve contains two parts. The Zone A shows the fluctuation energy absorbing behavior of the structure, which is the resistant of the sandwich panel core to a complete structure crashing. Moreover, the Zone B displays a linear normalized energy behavior via the normalized stresses of samples. According to Fig. 10(c), normalized energy behavior of 3D-ML-6 starts in higher levels of absorbed energy because of its better mechanical behavior and a broader range of borne stresses.

The 3D-RP curves show a noisy curve which could be due to the nature of the polymeric foams, the buckling phenomena of struts, and their fracture mechanism. Figure 10(d) shows the normalized energy via normalized strain for sandwich panel portions. The normalized energy of 3D-ML-6 starts to grow with a linier behavior with a minor slope. Additionally, by passing a transition region it continues to rise with a rapid gradient, and this phenomenon is clear in Figs. 10(d−f).

3.7 Specific energy absorption

Specific energy absorption (SEA), one of the critical parameters in the crashworthiness of foams and structures, is obtained from the force−displacement curve by the following equation and its relation with PPI is shown in Fig. 11.

$$\mathrm{SEA}=\frac{\int_0^{x_t}F(x)\,\mathrm{d}x}{m} \tag{5}$$

where x_t is the total crushed distance, F is the applied force at a certain x, and m is the total mass.

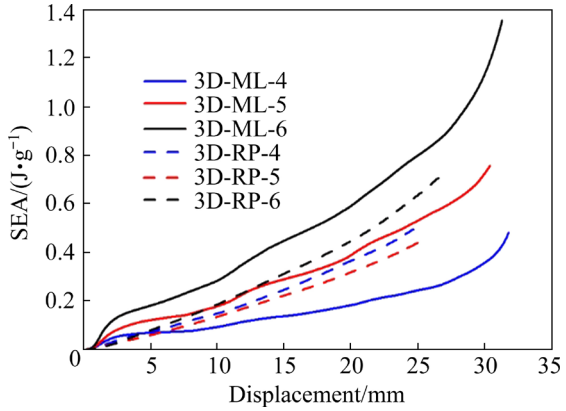

Fig. 11 SEA in relation with displacement for 3D-ML and 3D-RP structures

According to Fig. 11, the SEA increased with increasing PPI, and the 3D-ML-6 has the best SEA compared to other specimens.

4 Conclusions

(1) The yield strength of polymeric sandwich panels increased by increasing the PPI, 0.06, 0.07, and 0.12 MPa for 4, 5, and 6 PPI, respectively. The specific strength of the polymeric sandwich panels is 0.02, 0.01, and 0.03 MPa/g for 4, 5, and 6 PPI, respectively. The energy absorption density of these foams increased by increasing the PPI, 0.06, 0.07, and 0.12 MJ/m^3 for 4, 5, and 6 PPI, respectively.

(2) The yield strength of Ni/Ni−Cu/Ni coat reinforced polymeric sandwich panels increased by increasing the PPI, 0.64, 0.97, and 1.83 MPa for 4, 5, and 6 PPI, respectively. The specific strength of these sandwich panels is 0.05, 0.08, and 0.15 MPa/g for 4, 5, and 6 PPI, respectively. The energy absorption density of the Ni−Ni/Cu−Ni foams increased by increasing the PPI, 0.22, 0.36, and 0.67 MJ/m^3 for 4, 5, and 6 PPI, respectively.

(3) Among polymer and Ni/Ni−Cu/Ni reinforced samples, the best structures of this study were 3D-RP-6 for the polymeric type of cores and 3D-ML-6 for the reinforced type of cores. It can be said that the 50−60 μm multi-layer of deposited metal on the polymer sample increased the mass of 3D-RP-6 by 7.38 g. It is clear that at constraint strain (0.75), the multi-layer coat improved all properties of the polymeric samples by comparing 3D-RP-6 and 3D-ML-6. The yield strength reached 1.83 from 0.12 MPa (14 times superior), and the total absorbed energy of 3D-RP-6 also increased from 0.34 to 4.13 MJ/m^3 for 3D-RP-Ni-6 (12 times better). Furthermore, the specific energy absorption of the polymer sandwich panel also increased from 0.71 to 1.36 J/g for the nickel reinforced sandwich panel (two times more).

(4) The normalized energy plots via the normalized stress and the strain show that the coating of Ni/Ni−Cu/Ni shells could eliminate the noisy behavior of sandwich panels with polymeric foam cores.

CRediT authorship contribution statement

Mehrnoosh HOSSEINPOUR: Methodology, Validation, Investigation, Data Curation, Writing − Original Draft, Visualization; **Salar ROHANI NEJAD:**

Methodology, Software and computational design, Implementation of the computer code and supporting algorithms, Validation, Investigation, Data Curation, Visualization; **Seyyed Mohammad Hossein MIRBAGHERI:** Conceptualization, Methodology, Validation, Investigation, Resources, Writing − Review & editing, Supervision.

Declaration of competing interest

The authors declare that they have no known competing financial interests or personal relationships that could have appeared to influence the work reported in this paper.

Acknowledgments

The authors are very grateful to the financial supported from Rahyaft Advanced Sciences & Technologies knowledge-based company (No. RNAST.Co: 2021020713991115) and Mr. Arash Khiabani from Rahyaft Advanced Sciences & Technology for his technical support.

References

[1] FAIDZI M, ABDULLAH S, ABDULLAH M, AZMAN A, HUI D, SINGH S. Review of current trends for metal-based sandwich panel: Failure mechanisms and their contribution factors [J]. Engineering Failure Analysis, 2021, 123: 105302.

[2] MA Q, REJAB M, SIREGAR J, GUAN Z. A review of the recent trends on core structures and impact response of sandwich panels [J]. Journal of Composite Materials, 2021, 55: 2513−2555.

[3] WANG N Z, CHEN X, LI A, LI Y X, ZHANG H W, LIU Y. Three-point bending performance of a new aluminum foam composite structure [J]. Transactions of Nonferrous Metals Society of China, 2016, 26: 359−368.

[4] BAI R X, GUO J J, LEI Z K, LIU D, MA Y, YAN C. Compression after impact behavior of composite foam−core sandwich panels [J]. Composite Structures, 2019, 225: 111181.

[5] CHERNIAEV A. Modeling of hypervelocity impact on open cell foam core sandwich panels [J]. International Journal of Impact Engineering, 2021, 155: 103901.

[6] KUMAR S S, RAO M S, BALASUNDAR I, SINGH A K, RAGHU T, REDDY G M. Compressive behaviour of a nickel superalloy Superni 263 honeycomb sandwich panel [J]. Journal of Sandwich Structures & Materials, 2020, 22: 1426−1449.

[7] LV W T, LI D, DONG L. Study on blast resistance of a composite sandwich panel with isotropic foam core with negative Poisson's ratio [J]. International Journal of Mechanical Sciences, 2021, 191: 106105.

[8] GUO Y, CHEN C, WANG Q B, LIU M, CAO Y K, PAN Y M, TAN L M. Effect of porosity on mechanical properties of porous tantalum scaffolds produced by electron beam powder bed fusion [J]. Transactions of Nonferrous Metals Society of China, 2022, 32: 2922−2934.

[9] FAN S F, ZHANG T, KUN Y, FANG H J, XIONG H Q, DAI Y L, MA J J, JIANG D Y, ZHU H L. Compressive properties and energy absorption characteristics of open-cell nickel foams [J]. Transactions of Nonferrous Metals Society of China, 2017, 27: 117−124.

[10] BETTS C, BALINT D, LEE J, LIN J, LEE P. In situ microtensile testing and X-ray microtomography-based finite element modelling of open-cell metal foam struts and sandwich panels [J]. The Journal of Strain Analysis for Engineering Design, 2014, 49: 592−606.

[11] HUO X T, LIU H, LUO Q T, SUN G Y, LI Q. On low-velocity impact response of foam−core sandwich panels [J]. International Journal of Mechanical Sciences, 2020, 181: 105681.

[12] NEU T R, KAMM P H, von der ELTZ N, SEELIGER H W, BANHART J, GARCIA-MORENO F. Correlation between foam structure and mechanical performance of aluminium foam sandwich panels [J]. Materials Science and Engineering A, 2021, 800: 140260.

[13] QIN Q H, ZHANG J X, WANG Z J, LI H M, GUO D. Indentation of sandwich beams with metal foam core [J]. Transactions of Nonferrous Metals Society of China, 2014, 24: 2440−2446.

[14] RABIEI A, PORTANOVA M, MARX J, SCOTT C, SCHWANDT J. A study on puncture resistance of composite metal foam core sandwich panels [J]. Advanced Engineering Materials, 2020, 22: 2000693.

[15] SHUNMUGASAMY V C, MANSOOR B. Aluminum foam sandwich with density-graded open-cell core: Compressive and flexural response [J]. Materials Science and Engineering A, 2018, 731: 220−230.

[16] SMORYGO O, MIKUTSKI V, VAZHNOVA A, HANCHAROU V, TIKHOV S, JANAGAM V K, GOKHALE A A. Improving sintering kinetics and compositional homogeneity of Inconel 625 superalloy open-cell foams made by suspension impregnation method [J]. Transactions of Nonferrous Metals Society of China, 2021, 31: 2388−2401.

[17] BURTEAU A, BARTOUT J D, BIENVENU Y, FOREST S. On the creep deformation of nickel foams under compression [J]. Comptes Rendus Physique, 2014, 15: 705−718.

[18] ESCOBEDO J, DENNIS-KOLLER D, CERRETA E, PATTERSON B, BRONKHORST C, HANSEN B, TONKS D, LEBENSOHN R A. Effects of grain size and boundary structure on the dynamic tensile response of copper [J]. Journal of Applied Physics, 2011, 110: 033513.

[19] ZHANG Y, YANG X, LIAW P K. Alloy design and properties optimization of high-entropy alloys [J]. JOM, 2012, 64: 830−838.

[20] Standard ISO 13314:2016 (Edition 2). Mechanical Testing of Metals Ductility Testing Compression Test for Porous and Cellular Metals [S]. 2016.

[21] DAOUD A. Synthesis and characterization of novel ZnAl22 syntactic foam composites via casting [J]. Materials Science and Engineering A, 2008, 488: 281−295.

[22] FAN J H, ZHANG J J, WANG Z H, LI Z Q, ZHAO L M. Dynamic crushing behavior of random and functionally

graded metal hollow sphere foams [J]. Materials Science and Engineering A, 2013, 561: 352−361.
[23] LIU J A, YU S R, ZHU X Y, WEI M, LUO Y R, LIU Y H. Correlation between ceramic additions and compressive properties of Zn−22Al matrix composite foams [J]. Journal of Alloys and Compounds, 2009, 476: 220−225.
[24] MIRBAGHERI S M H, SALEHI M. Complementary and normalized energies during static and dynamic uniaxial deformation of single and multi-layer foam-filled tube [J]. Journal of Sandwich Structures & Materials, 2022, 24: 1470−1490.
[25] GONZÁLEZ NAVA M, CRUZ-RAMÍREZ A, SUAREZ ROSALES M Á, GUTIÉRREZ-PÉREZ V H, SÁNCHEZ-MARTÍNEZ A. Fabrication of aluminum alloy foams by using alternative thickening agents via melt route [J]. Journal of Alloys and Compounds, 2017, 698: 1009−1017.
[26] YOO C H, LEE S. Stability of structures: Principles and applications [M]. Amsterdam, Elsevier, 2011.

3D 打印和电沉积多层超轻夹层板的力学性能和能量吸收性能

Mehrnoosh HOSSEINPOUR, Salar ROHANI NEJAD, Seyed Mohammad Hossein MIRBAGHERI

Department of Materials and Metallurgical Engineering,
Amirkabir University of Technology, Hafez St., Tehran, 15875-4413, Iran

摘　要：研究由开孔聚合物和金属/聚合物泡沫芯制成的轻质夹层板的力学性能和能量吸收性能。通过结合聚合物树脂的增材制造和三层金属(Ni/Ni−Cu/Ni)的电沉积制备多层夹层板，每英寸孔数(PPI)为 4、5 和 6。测试样品在单轴压缩变形过程中的屈服强度，计算其能量吸收密度、互补能和比吸收能(SEA)。结果表明，与相同厚度的纯 Ni 和 Cu 夹层板相比，复合夹层板的性能有明显改善。增加 PPI 和金属层可提高力学性能和能量吸收性能，当 PPI 为 6 时，屈服强度(能量吸收密度)由聚合物夹层板的 0.12 MPa (0.12 MJ/m^3)提高到三层金属夹层板的 1.83 MPa (0.67 MJ/m^3)。对夹层板结构归一化能量的研究表明，夹层板具有可预测的塑性变形行为，多金属层改善了新型夹层板的力学性能。其能量吸收性能的显著增强可保证材料在不同行业的独特应用。

关键词：夹层板；能量吸收；金属泡沫；Voronoi 结构；增材制造；金属电层级

(Edited by Bing YANG)